Adhesive contact of an elastic semi-infinite solid with a rigid rough surface: strength of adhesion and contact instabilities

Z. Song, K. Komvopoulos

PII: S0020-7683(13)00434-4
DOI: http://dx.doi.org/10.1016/j.ijsolstr.2013.10.039
Reference: SAS 8172

To appear in: *International Journal of Solids and Structures*

Received Date: 2 August 2013
Revised Date: 30 October 2013

Please cite this article as: Song, Z., Komvopoulos, K., Adhesive contact of an elastic semi-infinite solid with a rigid rough surface: strength of adhesion and contact instabilities, *International Journal of Solids and Structures* (2013), doi: http://dx.doi.org/10.1016/j.ijsolstr.2013.10.039

Adhesive contact of an elastic semi-infinite solid with a rigid rough surface: strength of adhesion and contact instabilities

Z. Song, K. Komvopoulos*

Department of Mechanical Engineering, University of California, Berkeley, CA 94720, USA

Abstract

The effect of adhesion on the contact behavior of elastic rough surfaces is examined within the framework of the multi-asperity contact model of Greenwood and Williamson (1966), known as the GW model. Adhesive surface interaction is modeled by nonlinear springs with a force-displacement relation governed by the Lennard-Jones (LJ) potential. Constitutive models are presented for contact systems characterized by low and high Tabor parameters, exhibiting continuous (stable) and discontinuous (unstable) surface approach, respectively. Constitutive contact relations are obtained by integrating the force-distance relation derived from the LJ potential with a finite element analysis of single-asperity adhesive contact. These constitutive relations are then incorporated into the GW model, and the interfacial force and contact area of contacting rough surfaces are determined numerically. The development of attractive and repulsive forces at the contact interface and the occurrence of instantaneous surface contact (jump-in instability) yield a three-stage evolution of the contact area. It is shown that the adhesion parameter introduced by Fuller and Tabor (1975) governs the strength of adhesion of contact systems with a high Tabor parameter, whereas the strength of adhesion of contact systems with a low Tabor parameter is characterized by a new adhesion parameter, defined as the ratio of the surface roughness to the equilibrium interatomic distance. Applicable ranges of aforementioned adhesion parameters are interpreted in terms of the effective surface separation, obtained as the sum of the effective distance range of the adhesion force and the elastic deformation induced by adhesion. Adhesive contact of rough surfaces in the entire range of the Tabor parameter is discussed in terms of a generalized adhesion parameter, defined as the ratio of the surface roughness to the effective surface separation.

Keywords: Adhesion, Asperity, Contact instabilities, Elastic deformation, Rough surfaces, Strength of adhesion

*Corresponding author: Tel.: +1 510 642 2563; fax: +1 510 642 5539; e-mail: kyriakos@me.berkeley.edu

Submitted to the *International Journal of Solids and Structures* on August 2, 2013; revised manuscript submitted on September 24, 2013.

1. Introduction

Surface adhesion and roughness have attracted significant attention in contemporary contact mechanics studies. Because of the wide range of surface topology features, contact models based on simple geometrical configurations, such as a sphere in contact with a semi-infinite solid, do not yield accurate solutions of the real contact area and interfacial tractions. Among the first contact analyses to consider adhesion effects on solid contact deformation are those of Johnson et al. (1971) and Derjaguin et al. (1975), who introduced elastic contact models for two adhering spheres, known as the JKR and the DMT model, respectively. These models show that the pull-off force P_{off} at the instant of surface detachment is equal to $-(3/2)\pi R\Delta\gamma$ (JKR model) and $-2\pi R\Delta\gamma$ (DMT model), where R is the reduced radius of curvature ($R = [1/R_1 + 1/R_2]^{-1}$, where R_1 and R_2 are the radii of curvature of the two contacting spheres, respectively) and $\Delta\gamma$ is the work of adhesion ($\Delta\gamma = \gamma_1 + \gamma_2 - \gamma_{12}$, where γ_1 and γ_2 are the surface energies of the two spheres, respectively, and γ_{12} is the interfacial energy).

Adhesive elastic contacts can be characterized by the dimensionless Tabor parameter μ, defined as (Tabor, 1977):

$$\mu = \left[\frac{R\Delta\gamma^2}{E^{*2}\varepsilon^3}\right]^{1/3} \tag{1}$$

where $E^* = [(1-\nu_1^2)/E_1 + (1-\nu_2^2)/E_2]^{-1}$ is the effective elastic modulus (E and ν represent the elastic modulus and Poisson's ratio, respectively) and ε is the equilibrium interatomic distance. Tabor (1977) has argued that the JKR model is suitable for compliant spherical bodies with a large radius of curvature ($\mu > 5$), whereas the DMT model is more appropriate for stiff spherical bodies with a small radius of curvature ($\mu < 0.1$). Maugis (1992) used the Dugdale approximation to represent the adhesive stress at the contact interface and obtained P_{off} as a function of a dimensionless parameter λ ($\lambda = 1.16\mu$) in the transition range of the Tabor parameter bounded by the DMT and the JKR solutions. Carpick et al. (1999) derived a semi-empirical equation of P_{off} in terms of λ by using a curve-fitting method and numerical results obtained by Maugis (1992). Muller et al. (1980), Greenwood (1997), and Feng (2001)

used the Lennard-Jones (LJ) potential to model interfacial adhesion in elastic contacts and a self-consistent integration method to numerically analyze adhesive contact. The solution obtained from the latter approach represents a smooth transition between the DMT and the JKR solutions, but differs from that obtained by Maguis (1992) in the same range of the Tabor parameter. Using a curve-fitting method identical to that of Carpick et al. (1999), Wu (2008) obtained an equation of the dimensionless pull-off force $\bar{P}_{\mathrm{off}} = P_{\mathrm{off}}/2\pi R\Delta\gamma$ in terms of the Tabor parameter, given by

$$\bar{P}_{\mathrm{off}} = -\frac{1}{8}\left(7 + \frac{1 - 1.98\mu^{3/2}}{1 + 1.98\mu^{3/2}}\right) \tag{2}$$

where the negative sign in Eq. (2) indicates an attractive force. The aforementioned self-consistent integration method has been used in finite element analyses where interfacial adhesion was modeled by nonlinear spring elements obeying a force-displacement constitutive relation derived from the LJ potential (Du et al., 2007; Kadin et al., 2008; Song and Komvopoulos, 2011).

Despite of well-established theories of adhesive contact of elastic spheres or equivalent systems, the applicability of these models is limited because real surfaces are rough. One of the first contact models accounting for surface roughness effects is that of Greenwood and Williamson (1966), often referred to as the GW model. Modeling the rough surface by spherical asperities of identical radius of curvature and varied height, they developed a multiple-asperity framework, which allows for macroscopic contact parameters (e.g., real contact area and contact force) to be calculated by a numerical integration of an asperity-scale contact model. Ciavarella et al. (2008) assumed uniform contact pressure over the nominal contact area, which induces an increase in mean surface separation, and improved the GW model by including the effect of asperity interaction. Despite of significant differences between the later model and the original GW model for rough surfaces in close intimacy, they observed a good agreement between the original GW model and numerical results of three-dimensional fractal surfaces for mean surface separation larger than 1.5 times the surface roughness.

One of the first fundamental studies of adhesive contact between elastic rough surfaces is attributed to Fuller and Tabor (1975). Using the statistical rough-surface GW model and the JKR

approximation at the asperity level, they showed that the strength of adhesion of contacting rough surfaces decreases with the dimensionless adhesion parameter θ, given by

$$\theta = \frac{E^* \sigma^{3/2}}{R^{1/2} \Delta\gamma} = \left[\frac{\sigma}{R^{1/3} \Delta\gamma^{2/3} / E^{*2/3}}\right]^{3/2} \quad (3)$$

where σ is the root-mean-square (rms) surface roughness. The physical meaning of θ can be understood by considering that it represents the ratio of the surface roughness to the elastic deformation caused by adhesion at the instant of surface separation, as shown by the second form of Eq. (3). The strength of adhesion between a smooth rubber sphere and a hard rough surface, evaluated in terms of θ (Eq. (2)), has been found to be in good agreement with experimental results (Fuller and Tabor, 1975). Maugis (1996) used a similar approach and the DMT model to study the contact behavior of adhering asperities and observed a contribution of the adhesion force outside the contact region of interacting asperities to the total normal force. The existence of an adhesion force in most contact systems explains the finite friction force obtained with a zero or negative (adhesive) normal force and the higher friction of clean surfaces. Morrow et al. (2003) incorporated an improved Maugis solution, originally derived by Kim et al. (1998) for the transition range between the DMT and the JKR solutions, into the model of Fuller and Tabor (1975) and determined the adhesion force produced from non-contact and contact asperity regions in the entire range of λ.

Sahoo and Chowdhury (1996) developed an elastic adhesive contact model for rough surfaces that uses the Weierstrass-Mandelbrot function to describe fractal surfaces. This model was later improved by Mukherjee et al. (2004), who analyzed elastic-plastic deformation of adhering asperities by the finite element method. Experimental and analytical studies of Kesari et al. (2010) have shown that the force hysteresis observed in atomic force microscopy and nanoindentation measurements can be correlated to a series of asperity-contact instabilities attributable to adhesion and roughness effects. Kesari and Lew (2011) analyzed the compression of an elastic half-space by an axisymmetric rigid punch with random periodic undulations in the radial direction and observed multiple equilibrium contact regions during the loading and unloading phases by minimizing the potential energy of the system.

Although the previous studies have yielded important insight into the contact behavior of adhesive rough surfaces, the majority of these studies are either restricted to "hard" contact at the asperity scale (i.e., negligible adhesion forces between noncontacting asperities) or rely on the solution derived by Maguis (1992), which does not reproduce important physical phenomena, such as the contact instabilities due to instantaneous surface contact (jump-in) encountered with contact microprobes and suspended microstructures. The objective of this study was to develop an adhesive contact analysis of elastic rough surfaces, which models surface adhesion with nonlinear springs obeying a force-displacement law derived from the LJ potential, accounting for both JKR and DMT type of adhesive contacts at the asperity scale. Jump-in contact instabilities are identified by the sharp increase of the interfacial force or the instantaneous establishment of surface contact. The dependence of macrocontact instabilities in rough-surface contact on the Tabor parameter was found to differ from that of single-asperity contact observed in a previous study (Song and Komvopoulos, 2011). The effects of surface roughness and Tabor parameter on the strength of adhesion and the evolution of the interfacial force and the contact area are discussed in the context of numerical solutions. It is shown that the classical adhesion parameter of Fuller and Tabor (1975) only governs the strength of adhesion of compliant rough surfaces (high μ range). Thus, a new adhesion parameter is introduced for relatively stiff contact systems (low μ range). The applicable ranges of the aforementioned adhesion parameters are determined for three different characteristic length scales at the single-asperity and rough-surface levels and a generalized adhesion parameter is proposed for the entire range of the Tabor parameter.

2. Analysis of single-asperity contacts

Because contact between real (rough) surfaces comprises numerous microscopic asperity contacts, it is necessary to derive constitutive deformation relations that are applicable at the asperity level. The problem of two elastic spherical asperities in close proximity is equivalent to that of a rigid sphere of reduced radius of curvature R and an elastic half-space of effective elastic modulus E^*. In the presence of interfacial adhesive (attractive) pressure, the surface of the half-space deforms in the upward direction, as

shown schematically in Fig. 1. Song and Komvopoulos (2011) obtained the dimensionless elastic deflection at the center of the proximity region $\bar{h}_0 = h_0/\varepsilon$ by integrating the solution of a point surface force acting on an elastic half-space (Boussinesq, 1885), i.e.,

$$\bar{h}_0 = \int_0^\infty \frac{p(r)}{\pi E^* r} 2\pi r dr = \sqrt{2}\pi\mu^{3/2}\left[\bar{x}_0^{-5/2} - \frac{2145}{4096}\bar{x}_0^{-17/2}\right] \quad (4)$$

where $p(r)$ is the adhesive pressure, derived from the LJ potential, and $\bar{x}_o = x_o/\varepsilon$ is the dimensionless minimum surface gap. Consequently, the dimensionless minimum surface separation at $r = 0$, defined as $\bar{\delta}_o = \delta_o/\varepsilon$, can be expressed as

$$\bar{\delta}_o = \bar{x}_o + \bar{h}_o \quad (5)$$

Analytical and finite element results (Song and Komvopoulos, 2011) show that jump-in is not observed for $\mu < 0.5$ and the interfacial force P and contact area A vary continuously as the two asperities approach each other (Fig. 2(a)) and 2(c), respectively), while for $\mu > 0.5$ jump-in commences, as evidenced by the abrupt increase of the interfacial force (tensile) (Fig. 2(b)) and the instantaneous establishment of surface contact (Fig. 2(d)). The critical (minimum) surface separation corresponding to the maximum adhesion force $P_{\max}$ during the approach of the surfaces and the inception of initial contact (i.e., the surface separation at the transition instant from zero to nonzero contact area) are denoted by δ_{oc} and δ_o^*, respectively (Fig. 2). The definition of the contact area may appear to be controversial because "hard" contact, such as that considered in classical contact mechanics of adhesionless surfaces, is not possible in the present analysis due to the repulsive term in the LJ potential (Greenwood, 1997; Feng, 2000, 2001). Thus, for consistency with classical contact mechanics, the contact area is defined as the area of compressive normal traction. For $\mu < 0.5$, the contact area at the instant of $P_{\max}$ can be either zero or nonzero. In particular, for very low μ values, $P_{\max}$ is encountered before contact (i.e., $\delta_{oc} > \delta_o^*$), for moderate μ values less than 0.5, contact commences before the occurrence of $P_{\max}$ (i.e., $\delta_{oc} < \delta_o^*$) (Figs. 2(a) and 2(c)), and for $\mu > 0.5$, both $P_{\max}$ and initial contact are encountered at the instant of jump-in (i.e., $\delta_{oc} = \delta_o^*$) (Figs. 2(b) and 2(d)).

Fig. 3 shows the dimensionless contact radius $\bar{a}_c = a_c/(\varepsilon R)^{1/2}$ corresponding to the critical minimum surface separation δ_{oc} as a function of the Tabor parameter. Discrete data points represent numerical results obtained using a previous finite element model of adhesive contact (Song and Komvopoulos, 2011). Curve fitting of the numerical data yields

$$\bar{a}_c = 0 \qquad (\mu < 0.19) \tag{6a}$$

$$\bar{a}_c = 0.83\,(\mu - 0.19)^{1/2} \qquad (\mu \geq 0.19) \tag{6b}$$

Eqs. (6a) and (6b) indicate that, for $\mu < 0.19$, $P_{\max}$ occurs before the establishment of surface contact (i.e., $\delta_{oc} > \delta_o^*$), while for $\mu \geq 0.19$, contact is established either before or upon the occurrence of $P_{\max}$ (i.e., $\delta_{oc} < \delta_o^*$), with the contact radius given by Eq. (6b). It is noted that Eq. (6b) is the first relation to yield the contact area at the instant of $P_{\max}$ in terms of the Tabor parameter, and its validity is confirmed by favorable comparisons with analytical solutions obtained for large μ values. For example, for $\mu > 5$, Eq. (6b) yields $\bar{a}_c \approx 0.83\mu^{1/2}$, which is in excellent agreement with the solution derived from JKR theory, $\bar{a}_c \approx 0.88\mu^{1/2}$ (Eq. (A9) in Appendix A).

Considering the significant effect of the jump-in instability on the evolution of the interfacial force and the contact area, two different sets of constitutive relations of adhesive asperity contacts must be derived – one set for continuous elastic contact and another set for discontinuous elastic contact due to the occurrence of the jump-in instability. Moreover, because of the transition from attractive- to repulsive-dominant contact behavior encountered with the decrease of the surface separation, different constitutive relations must be derived for the surface separation ranges of attractive and repulsive dominant force, i.e., $\delta_o \geq (\delta_{oc}, \delta_o^*)$ and $\delta_o < (\delta_{oc}, \delta_o^*)$, respectively.

2.1. Constitutive relations for the surface separation range of dominant attractive force

2.1.1. Elastic adhesive contacts not exhibiting jump-in instability

In the absence of the jump-in instability ($\mu < 0.5$), the interfacial force P increases continuously from zero (large δ_o) to a maximum adhesion force $P_{\max}$ with the decrease of δ_o to a critical value δ_{oc} (Fig. 2(a)). Fig. 4 shows the dimensionless critical minimum surface separation $\bar{\delta}_{oc}$ $(= \delta_{oc}/\varepsilon)$

corresponding to $P_{\max}$ as a function of μ for adhesive elastic contacts that do not exhibit jump-in. From a linear fit through the numerical results (discrete data points), obtained with a previous finite element model (Song and Komvopoulos, 2011), it is found that

$$\bar{\delta}_{oc} = 1 + 0.922\mu \tag{7}$$

Assuming small deformation in the elastic half-space for $\bar{\delta}_o > \bar{\delta}_{oc}$, the dimensionless interfacial force $\bar{P} = P/2\pi R\Delta\gamma$, obtained by integrating the surface traction applied to the undeformed surface of the half-space (Boussinesq, 1885), is given by

$$\bar{P} = \frac{1}{-2\pi R\varepsilon\Delta\gamma}\int_0^\infty p(r)2\pi r dr = \frac{1}{-2\pi R\varepsilon\Delta\gamma}\int_0^\infty \left[\frac{8\Delta\gamma}{3\varepsilon}\left(\frac{\varepsilon}{\delta_o + r^2/2R}\right)^{-3} - \left(\frac{\varepsilon}{\delta_o + r^2/2R}\right)^{-9}\right]2\pi r dr =$$

$$= \frac{1}{3}\left(\bar{\delta}_o^{-8} - 4\bar{\delta}_o^{-2}\right) \qquad \left(\bar{\delta}_o \geq \bar{\delta}_{oc}\right) \tag{8}$$

Applying the boundary condition $\bar{P}\left(\bar{\delta}_o = \bar{\delta}_{oc}\right) = \bar{P}_{\max} = P_{\max}/2\pi R\Delta\gamma$, where $P_{\max}$ is given by Eq. (2), because for elastic adhesive contact $P_{\max} = P_{\text{off}}$, while retaining the force-distance proportionality that is intrinsic of the LJ potential (i.e.,$\bar{P} \propto \bar{\delta}_o^{-8} - 4\bar{\delta}_o^{-2}$), Eq. (8) can be modified as

$$\bar{P} = \left[\frac{\bar{\delta}_o^{-8} - 4\bar{\delta}_o^{-2}}{\bar{\delta}_{oc}^{-8} - 4\bar{\delta}_{oc}^{-2}}\right]\bar{P}_{\max} \qquad \left(\bar{\delta}_o \geq \bar{\delta}_{oc}\right) \tag{9}$$

Fig. 5 shows analytical solutions (Eq. (9)) and finite element method (FEM) results (Song and Komvopoulos, 2011) of the dimensionless interfacial force $\bar{P}$ versus the dimensionless minimum surface separation $\bar{\delta}_o$ at $r = 0$ for μ in the range of 0.091–0.425. The good agreement between analytical and FEM results validates Eq. (9).

Because the minimum surface separation occurs at $r = 0$, δ_o^* is obtained for $\bar{x}_0 = 1$. Thus, the following equation of the dimensionless critical minimum surface separation $\bar{\delta}_o^*$ at the instant of initial contact is obtained by substituting $\bar{x}_0 = 1$ into Eqs. (4) and (5):

$$\bar{\delta}_o^* = 1 + 2.116\,\mu^{3/2} \tag{10}$$

For the dimensionless contact area, defined as $\bar{A} = A/\varepsilon R$, it follows that

$$\bar{A} = 0 \quad (\bar{\delta}_o \geq \bar{\delta}_o^*) \tag{11}$$

A transition value of the Tabor parameter equal to 0.19 is obtained by equating Eq. (7) with Eq. (10). For $\mu < 0.19$, $\bar{\delta}_o^* < \bar{\delta}_{oc}$, implying that $\bar{A} = 0$ at the instant of $\bar{P}_{\max}$, whereas for $0.19 < \mu < 0.5$, a finite contact area is established before the occurrence of $\bar{P}_{\max}$, which is in excellent agreement with the predictions of Eqs. (6a) and (6b).

2.1.2. Elastic adhesive contacts exhibiting jump-in instability

As mentioned earlier, when $\mu > 0.5$, initial contact and $P_{\max}$ occur simultaneously at the instant of jump-in (i.e., $\delta_{oc} = \delta_o^*$). From curve fitting the jump-in part of the contact instability equation (Song and Komvopoulos, 2011), the dimensionless critical surface gap $\bar{x}_{oc} = x_{oc}/\varepsilon$ at the instant of jump-in is obtained as

$$\bar{x}_{oc} = -0.3 + 2.2\mu^{2/5} \tag{12}$$

Substitution of Eq. (12) into Eqs. (4) and (5) yields

$$\bar{\delta}_o^* = \bar{\delta}_{oc} = -0.3 + 2.2\mu^{2/5} + \sqrt{2}\pi\mu^{3/2}\left[\left(-0.3 + 2.2\mu^{2/5}\right)^{-5/2} - \frac{2145}{4096}\left(-0.3 + 2.2\mu^{2/5}\right)^{-17/2}\right] \tag{13}$$

For $\bar{\delta}_o \geq \bar{\delta}_{oc} = \bar{\delta}_o^*$, elastic deformation can be ignored as negligibly small in comparison to the relatively large surface separation. Thus, an approximate expression of the interfacial force can be derived by integrating the surface traction for the undeformed configuration of the half-space, i.e.,

$$\bar{P} = \frac{1}{-2\pi R\varepsilon\Delta\gamma}\int_0^\infty p(r)\,2\pi r dr =$$

$$= \frac{1}{-2\pi R\varepsilon\Delta\gamma}\int_0^\infty \left[\frac{8\Delta\gamma}{3\varepsilon}\left(\frac{\varepsilon}{\delta_o + r^2/2R}\right)^{-3} - \left(\frac{\varepsilon}{\delta_o + r^2/2R}\right)^{-9}\right]2\pi r dr = \frac{1}{3}\left(\bar{\delta}_o^{-8} - 4\bar{\delta}_o^{-2}\right) \tag{14}$$

Because the critical minimum surface separation is larger than the equilibrium interatomic distance, before the commencement of jump-in the surface traction is attractive everywhere and the contact area is zero, i.e.,

$$\bar{A} = 0 \quad (\bar{\delta}_o \geq \bar{\delta}_o^*) \tag{15}$$

At the instant of jump-in ($\bar{\delta}_o = \bar{\delta}_{oc} = \bar{\delta}_o^*$), the interfacial force increases instantaneously from a value given by Eq. (15) to a value given by Eq. (2), with the simultaneous abrupt formation of a contact area of dimensionless radius $\bar{a}_c$ (Eq. (6b)).

2.2. Constitutive relations for the surface separation range of dominant repulsive force

The decrease of the minimum surface separation δ_o below δ_{oc} and δ_o^* leads to the dominance of the repulsive term in the LJ potential and the dependence of the deformation behavior on the elastic material properties. The evolution of the interfacial force and the contact area was analyzed with a previous FEM model of adhesive contact (Song and Komvopoulos, 2011), using μ in the range of 0.091 (no jump-in) to 1.971 (jump-in). Figs. 7(a) and 7(b) show the dimensionless interfacial force $(P - P_{\max})/(4E^* R^2/3)$ and the contact area $(A - \pi a_c^2)/\pi R^2$ as functions of the dimensionless minimum surface separation $(\delta_{oc} - \delta_o)/R$ and $(\delta_o^* - \delta_o)/R$, respectively. The good agreement between FEM results and analytical (Hertz) solutions suggests that the jump-in instability does not affect the constitutive relations in the surface separation range dominated by the repulsive force. Hence, the following constitutive relations hold after the occurrence of $P_{\max}$ and the establishment of initial contact:

(a) For adhesive elastic contacts that do not exhibit jump-in ($\mu < 0.5$):

$$\bar{P} = \bar{P}_{\max} + \bar{P}_H = \bar{P}_{\max} + \frac{1}{2\pi R\Delta\gamma}\left(\frac{4}{3}E^* R^{1/2}\right)(\delta_{oc} - \delta_o)^{3/2} = \bar{P}_{\max} + \frac{2}{3\pi}\left(\frac{\bar{\delta}_{oc} - \bar{\delta}_o}{\mu}\right)^{3/2} \quad (\bar{\delta}_o < \bar{\delta}_{oc}) \quad (16)$$

$$\bar{A} = \bar{A}_H = \frac{A}{\varepsilon R} = \frac{\pi R(\delta_o^* - \delta_o)}{\varepsilon R} = \pi\left(\bar{\delta}_o^* - \bar{\delta}_o\right) \qquad (\bar{\delta}_o < \bar{\delta}_o^*) \quad (17)$$

(b) For adhesive elastic contacts that exhibit jump-in ($\mu > 0.5$):

$$\bar{P} = \bar{P}_{\max} + \bar{P}_H = \bar{P}_{\max} + \frac{1}{2\pi R\Delta\gamma}\left(\frac{4}{3}E^* R^{1/2}\right)(\delta_{oc} - \delta_o)^{3/2} = \bar{P}_{\max} + \frac{2}{3\pi}\left(\frac{\bar{\delta}_{oc} - \bar{\delta}_o}{\mu}\right)^{3/2} \quad (\bar{\delta}_o < \bar{\delta}_{oc}) \quad (18)$$

$$\bar{A} = \pi\bar{a}_c^2 + \bar{A}_H = \pi\bar{a}_c{}^2 + \frac{\pi R(\delta_o^* - \delta_o)}{\varepsilon R} = \pi\left[0.69(\mu - 0.19) + \bar{\delta}_o^* - \bar{\delta}_o\right] \qquad \left(\bar{\delta}_o < \bar{\delta}_o^*\right) \quad (19)$$

where subscript *H* denotes Hertz analysis.

3. Contact analysis of elastic rough surfaces

3.1. Rough surface model

Fig. 8 shows a cross-sectional schematic of the equivalent system of two rough surfaces consisting of a rigid rough surface and a flat elastic half-space at a mean surface separation d from the rough surface. The rough surface is represented by the GW model, consisting of uniformly distributed spherical asperities of fixed radius of curvature R, area density η, and randomly varying height z. The topography of an isotropic rough surface can be uniquely defined by R, η, and the standard deviation of the surface heights, referred to as the rms surface roughness σ. The ratio of the standard deviation of the asperity heights σ_s to the surface roughness σ, denoted by ω, can be expressed as (McCool, 1986)

$$\omega = \frac{\sigma_s}{\sigma} = \left[1 - \frac{3.717 \times 10^{-4}}{(\sigma R \eta)^2}\right]^{1/2} \tag{20}$$

The probability of an asperity height to be between z and $z + dz$ is equal to $\phi(z)dz$, where $\phi(z)$ is the asperity height distribution function, described by a normal probability density function, which in dimensionless form can be written as

$$\tilde{\phi}(\tilde{z}) = \frac{\omega}{\sqrt{2\pi}} \exp\left(-\frac{\omega^2 \tilde{z}^2}{2}\right) \tag{21}$$

where $\tilde{z} = z/\sigma$. (Hereafter, the symbol ~ over a parameter denotes normalization by σ.) For a rigid rough surface of asperity area density η and apparent contact area A_o, the total number of potentially contacting asperities is $N = A_o\eta$. Because all the asperities possess the same radius of curvature, they are characterized by the same Tabor parameter.

3.2. Constitutive contact relations for rough elastic surfaces not exhibiting jump-in instabilities

For rough elastic surfaces comprising asperity contacts that do not exhibit jump-in contact instabilities (i.e., $\mu < 0.5$), the numbers of asperity contacts in the surface separation range dominated by attraction ($\tilde{d} - \tilde{z} \geq \tilde{\delta}_{oc}$) and repulsion ($\tilde{d} - \tilde{z} < \tilde{\delta}_{oc}$) N_1 and N_2, respectively, where $\tilde{d} = d/\sigma$ is the dimensionless mean surface separation (Fig. 8) and $\tilde{\delta}_{oc} = \delta_{oc}/\sigma$, are given by

$$N_1 = N \int_{-\infty}^{\tilde{d}-\tilde{\delta}_{oc}} \tilde{\phi}(\tilde{z}) d\tilde{z} \tag{22a}$$

and

$$N_2 = N\int_{\tilde{d}-\tilde{\delta}_{oc}}^{\infty}\tilde{\phi}(\tilde{z})d\tilde{z} \tag{22b}$$

where $\tilde{\delta}_{oc} = \delta_{oc}/\sigma$ and δ_{oc} is given by Eq. (7).

Using Eqs. (2), (9), (16), (22a), and (22b), the dimensionless total interfacial force $\bar{F}$ can be expressed as

$$\bar{F} = \frac{F}{2\pi R A_0 \Delta\gamma\eta} = \int_{-\infty}^{\tilde{d}-\tilde{\delta}_{oc}} -\frac{1}{8}\left(7+\frac{1-1.98\mu^{3/2}}{1+1.98\mu^{3/2}}\right)\frac{4\left[\frac{(\tilde{d}-\tilde{z})\sigma}{\varepsilon}\right]^{-2}-\left[\frac{(\tilde{d}-\tilde{z})\sigma}{\varepsilon}\right]^{-8}}{4\bar{\delta}_{oc}^{-2}-\bar{\delta}_{oc}^{-8}}\tilde{\phi}(\tilde{z})d\tilde{z}$$

$$+\int_{\tilde{d}-\tilde{\delta}_{oc}}^{+\infty}\left[-\frac{1}{8}\left(7+\frac{1-1.98\mu^{3/2}}{1+1.98\mu^{3/2}}\right)+\frac{2}{3\pi}\left(\frac{\sigma}{\mu\varepsilon}\right)^{3/2}\left[\tilde{z}-\left(\tilde{d}-\tilde{\delta}_{oc}\right)\right]^{3/2}\right]\tilde{\phi}(\tilde{z})d\tilde{z} \tag{23}$$

The numbers of noncontacting and contacting asperities N_3 and N_4, respectively, are given by

$$N_3 = N\int_{-\infty}^{\tilde{d}-\tilde{\delta}_o^*}\tilde{\phi}(\tilde{z})d\tilde{z} \tag{24a}$$

and

$$N_4 = N\int_{\tilde{d}-\tilde{\delta}_o^*}^{\infty}\tilde{\phi}(\tilde{z})d\tilde{z} \tag{24b}$$

where $\tilde{\delta}_o^* = \delta_o^*/\sigma$ and δ_o^* is given by Eq. (10).

Using Eqs. (10), (17), (24a), and (24b), the dimensionless total contact area $\bar{S}$ can be expressed as

$$\bar{S} = \frac{S}{RA_0\eta\varepsilon} = \int_{\tilde{d}-\tilde{\delta}_o^*}^{+\infty}\pi\left(\frac{\sigma}{\varepsilon}\right)\left[\tilde{z}-\left(\tilde{d}-\tilde{\delta}_o^*\right)\right]\tilde{\phi}(\tilde{z})d\tilde{z} \tag{25}$$

3.3. Constitutive contact relations for rough elastic surfaces exhibiting jump-in instabilities

For asperity contacts demonstrating jump-in contact instabilities ($\mu > 0.5$), all asperities in the surface separation range dominated by attraction are not in contact, whereas all asperities in the surface separation range dominated by repulsion are in contact because $\delta_{oc} = \delta_o^*$. Thus, the corresponding asperity numbers are given by

$$N_5 = N\int_{-\infty}^{\tilde{d}-\tilde{\delta}_{oc}}\tilde{\phi}(\tilde{z})d\tilde{z} \tag{26a}$$

and

$$N_6 = N\int_{\tilde{d}-\tilde{\delta}_{oc}}^{\infty}\tilde{\phi}(\tilde{z})d\tilde{z} \tag{26b}$$

where $\tilde{\delta}_{oc}$ is obtained from Eq. (16).

Using Eqs. (2), (14), (18), (26a), and (26b), the dimensionless total interfacial force $\bar{F}$ can be written as

$$\bar{F} = \frac{F}{2\pi R A_0 \Delta\gamma\eta} = \int_{-\infty}^{\tilde{d}-\tilde{\delta}_{oc}} \frac{1}{3}\left[-4\left[\frac{(\tilde{d}-\tilde{z})\sigma}{\varepsilon}\right]^{-2} + \left[\frac{(\tilde{d}-\tilde{z})\sigma}{\varepsilon}\right]^{-8}\right]\tilde{\phi}(\tilde{z})d\tilde{z}$$
$$+\int_{\tilde{d}-\tilde{\delta}_{oc}}^{+\infty}\left[-\frac{1}{8}\left(7+\frac{1-1.98\mu^{3/2}}{1+1.98\mu^{3/2}}\right)+\frac{2}{3\pi}\left(\frac{\sigma}{\mu\varepsilon}\right)^{3/2}\left[\tilde{z}-\left(\tilde{d}-\tilde{\delta}_{oc}\right)\right]^{3/2}\right]\tilde{\phi}(\tilde{z})d\tilde{z} \tag{27}$$

From Eqs. (15), (16), (26a), and (26b), the dimensionless total contact area $\bar{S}$ can be obtained as

$$\bar{S} = \frac{S}{RA_0\eta\varepsilon} = \int_{\tilde{d}-\tilde{\delta}_o^*}^{+\infty}\pi\left[0.69(\mu-0.19)+\left[\tilde{z}-\left(\tilde{d}-\tilde{\delta}_o^*\right)\right]\left(\frac{\sigma}{\varepsilon}\right)\right]\tilde{\phi}(\tilde{z})d\tilde{z} \tag{28}$$

4. Results and discussion

4.1. Effect of adhesion-induced instabilities at the asperity level on the contact behavior of rough surfaces

Figs. 9(a) and 9(b) show the dimensionless total interfacial force $\bar{F}$ and the total contact area $\bar{S}$ of different rough surfaces as functions of the dimensionless mean surface separation $\tilde{d}$, respectively, for fixed surface roughness (σ = 2 nm) and μ varied in the range of 0.5–46.9 by changing the effective elastic modulus of the semi-infinite solid E^*. Since R/ε was fixed at a relatively high value, i.e., R/ε > 300, the Derjaguin approximation still holds and μ is the only governing parameter of elastic adhesive contact (Greenwood, 2009). As expected, lower values of the Tabor parameter characterize stiffer contact systems. Differences in the adhesive contact behavior between a single asperity and a rough surface can be examined by considering the variation of the interfacial force for μ = 10. (The inset of Fig. 9(a) shows a magnified plot of the interfacial force versus the mean surface separation for μ = 10.) It can be seen that the dimensionless maximum adhesive force $\bar{F}_{\max}$ obtained for μ = 10 is significantly less than 0.75, which

is the value predicted by the JKR model (single-asperity contact), and jump-in is not encountered despite that $\mu > 0.5$, which is the critical Tabor parameter for jump-in to occur in single-asperity adhesive contacts (Song and Komvopoulos, 2011).

Fig. 9(b) shows three distinct surface separation ranges of the evolution of the contact area. In the high range of mean surface separation, contact does not occur (range of zero contact area) and the interfacial force is very low and attractive because the surfaces are sufficiently apart. The critical surface separation for initial contact increases with the Tabor parameter due to the enhancement of jump-in contact at the asperity level (Eq. (13)). In the intermediate range of mean surface separation, the contact area increases nonlinearly as the surfaces approach closer, especially for higher μ values. In this range, asperities on the rough surface jump into contact with the elastic half-space, causing abrupt surface contact and the rapid growth of the contact area. The evolution of the contact area in the intermediate distance range is more pronounced for contact systems characterized by high μ values, implying an enhancement of the jump-in instabilities with increasing Tabor parameter. In addition, the rate of increase of the contact area (slope of $\bar{S}$ curves) also increases with the Tabor parameter (Eq. (6b)). In the low range of mean surface separation, the contact area increases linearly with the decrease of the mean surface separation at a rate independent of μ. In this range, the contact behavior is dominated by the repulsive term of the LJ potential and the linear response of the contact area is independent of μ and is accurately described by Hertz theory (Eq. (19)). The observed evolution of the contact area, particularly in the intermediate distance range, suggests that even though jump-in instabilities at the asperity level are not reflected in the interfacial force response (Fig. 9(a)), they affect the contact behavior. This phenomenon has not been observed in any of the previous studies, which are not based on constitutive models accounting for jump-in instabilities at the asperity scale. Therefore, it is necessary for constitutive contact models of adhesive rough surfaces to account for such contact instabilities. In addition, Fig. 9(b) shows that contact instabilities occur in the range $2\sigma < d < 5\sigma$, indicating a low interfacial force and a very small

fraction of contacting asperities, which implies that the GW model is still applicable (Ciavarella et al., 2008).

4.2. Effect of surface roughness on strength of adhesion

Fig. 10 shows the dimensionless maximum attractive force between rough surfaces $\bar{F}_{\max}$, hereafter referred to as the strength of adhesion, as a function of the surface roughness σ for μ = 0.1, 1.0, and 10. All three curves show the same general trend, i.e., an enhancement of the strength of adhesion with decreasing surface roughness. For a given surface roughness, the strength of adhesion increases with the Tabor parameter. The critical surface roughness for zero strength of adhesion also increases with the Tabor parameter, implying more pronounced adhesion effects with compliant surfaces. This is in agreement with the adhesion parameter θ of Fuller and Tabor (1975), which predicts a higher strength of adhesion for smoother and more compliant surfaces (Eq. (2)).

4.3. Effect of the Tabor parameter on the strength of adhesion

Fig. 11 shows the variation of the strength of adhesion $\bar{F}_{\max}$ with the Tabor parameter μ for σ = 0.5, 1.0, and 2.0 nm. Despite of the quantitative differences among the three curves, $\bar{F}_{\max}$ increases asymptotically with the Tabor parameter to 0.75, which is the value of $\bar{P}_{\text{off}}$ predicted by the JKR theory. This implies that the adhesive contact behavior of rough surfaces characterized by a high value of μ (e.g., $\mu > 10$) is fairly analogous to that of a single-asperity contact. This finding is consistent with the decreasing effect of surface roughness on the strength of adhesion observed with the increase of the Tabor parameter in Fig. 10 and confirmed by the asymptotic solution $\bar{F}_{\mu\to\infty} \to 0.75$ obtained from Eq. (27), implying a negligible roughness effects for highly compliant contacting surfaces. It is also noted that, for a given roughness, $\bar{F}_{\max}$ decreases sharply in the range $0.1 < \mu < 10$, asymptotically approaching to a small value that decreases with the surface roughness.

4.4. New adhesion parameter and effective surface separation

Numerical results of the strength of adhesion $\bar{F}_{\max}$ shown in Fig. 12(a) for θ = 0.2, 1.0, and 5.0 and σ in the range of 0–150 nm indicate that the adhesion parameter θ controls the strength of adhesion only for low θ values and/or high σ values, i.e., high range of Tabor parameter. The results shown in Fig. 12(b) provide further evidence that θ is a governing parameter of the strength of adhesion only in the high range of the Tabor parameter, in agreement by experiments with a smooth rubber sphere pressed into contact with a rough surface (Greenwood and Williamson, 1966). Therefore, a different adhesion parameter must be used to describe the strength of adhesion in the low range of the Tabor parameter.

Fig. 13 shows the strength of adhesion $\bar{F}_{\max}$ as a function of the Tabor parameter for new adhesion parameter $\zeta = \sigma/\varepsilon$ equal to 0.2. 0.5, and 1.0. The results indicate that ζ is a governing parameter of the strength of adhesion in the low μ range. Thus, because $\mu\varepsilon = (R\Delta\gamma^2/E^{*2})^{1/3}$ represents the elastic deformation caused by adhesion and ε characterizes the effective range of the adhesion force, a generalized adhesion parameter, defined as $\xi \sim \sigma/(\mu+1)\varepsilon$, can be used for the entire range of the Tabor parameter. Surface roughness σ characterizes the variation in the separation distance between individual asperities and the undeformed half-space (stress-free state), while asperity elastic deformation induced by adhesion is on the order of $\mu\varepsilon$ and the effective range of the adhesion force is on the order of ε. Therefore, the effective surface separation between individual asperities and the elastically deformed half-space is on the order of $(\mu+1)\varepsilon$, below which the adhesion force significantly affects the contact behavior. The asperity fraction in the range of surface separation dominated by the attractive force decreases with the surface roughness and increases with the effective surface separation.

The adhesion parameters θ and ζ represent asymptotic values of the general adhesion parameter ξ. For $\mu \gg 1$, the effective surface separation is controlled by adhesion-induced elastic deformation of the asperities and $\xi \to \sigma/\mu\varepsilon = \theta^{2/3}$, in agreement with the finding that θ governs the strength of adhesion of contact systems characterized by a high Tabor parameter (Fig. 12). Alternatively, for $\mu \ll 1$, the effective surface separation is controlled by the effective range of the adhesion force and $\xi \to \sigma/\varepsilon = \zeta$, in

agreement with the observation that ζ governs the strength of adhesion of contact systems characterized by a low Tabor parameter (Fig. 13).

The present analysis is applicable to homogeneous semi-infinite solids and rough surfaces, i.e., it accounts for contact instabilities both at asperity and macroscopic scales. However, most real surfaces are not clean and may contain a thin surface layer of absorbed contaminants or a native oxide film, depending on the surface material and its environment. The current analysis can easily be modified to model such surfaces by accordingly adjusting the interface work of adhesion and replacing the constitutive equations developed at the asperity scale for an elastic semi-infinite solid by those of an elastic layered medium (Ye and Komvopoulos, 2003; Komvopoulos and Gong, 2007). However, the contact problem may be further complicated by adhesion-induced delamination of an oxide or contaminant surface layer (Song and Komvopoulos, 2013).

5. Conclusions

Adhesive contact of elastic rough surfaces was examined within the framework of the GW rough surface model, modified to include contact instabilities (jump-in) at the asperity level. Constitutive relations of the interfacial force and the contact area of single-asperity contacts demonstrating continuous ($\mu < 0.5$) and discontinuous ($\mu > 0.5$) approach paths were obtained in the distance range of attractive- and repulsive-dominant surface force. These relations were incorporated into the GW rough-surface model, and the interfacial force and contact area were expressed in terms of important parameters, such as surface separation, asperity radius, asperity area density, surface roughness, effective elastic modulus, surface energy, equilibrium interatomic distance, and the Tabor parameter.

Rough surface contact demonstrated a three-stage behavior with decreasing mean surface separation: (1) zero contact area, (2) nonlinear and rapid increase of the contact area caused by jump-in instabilities at the asperity level (particularly for surfaces characterized by high μ values), and (3) linear increase of the contact area (Hertz-like behavior) independent of μ. The strength of adhesion decreased

with increasing surface roughness and generally increased with μ, approaching asymptotically to the value predicted by the JKR contact model of elastic spheres, implying a negligible surface roughness effect for $\mu \gg 1$. However, for $\mu \ll 1$, the strength of adhesion approached asymptotically to a very low value, which increased with decreasing surface roughness.

The adhesion parameter θ proposed by Fuller and Tabor (1975) was shown to govern the strength of adhesion of surfaces characterized by high μ values. A new adhesion parameter ζ, defined as the ratio of the surface roughness to the equilibrium interatomic distance, was shown to describe the strength of adhesion of rough surfaces characterized by low μ values. Differences between θ and ζ parameters were interpreted in terms of the effective surface separation, defined as the sum of the effective distance range of the adhesion force and the elastic deformation of asperities caused by adhesion. It was shown that the strength of adhesion can be characterized over the entire range of the Tabor parameter by a generalized adhesion parameter ξ, defined as the ratio of the surface roughness and the effective surface separation, with θ and ζ representing asymptotic values in the high- and low-ranges of the Tabor parameter, respectively.

Appendix A. Contact area at the maximum adhesion force derived from the JKR theory

In the JKR theory, the Hertzian equation of the contact radius a, modified to include the effect of surface energy, is given by (Johnson et al., 1971)

$$a = \left[\frac{3R}{4E^*}\left[P + 3\pi R\Delta\gamma + \{6\pi R\Delta\gamma P + (3\pi R\Delta\gamma)^2\}^{1/2}\right]\right]^{1/3} \quad \text{(A1)}$$

Substitution of $P = -(3/2)\pi R\Delta\gamma$ into Eq. (A1) leads to the following equation of the contact radius at the instant of $P_{\max}$:

$$a = \left[\frac{9\pi R^2\Delta\gamma}{8E^*}\right]^{1/3} \quad \text{(A2)}$$

Using the same normalization scheme, i.e., $\bar{a} = a/(\varepsilon R)^{1/2}$, Eq. (A2) can be written in dimensionless form as follows

$$\bar{a} = \left(\frac{9\pi}{8}\right)^{1/3} \mu^{1/2} \tag{A3}$$

The contact radius given by Eq. (A3) consists of regions with compressive and tensile surface tractions, whereas in Eq. (6b) the contact radius is defined as the region of compressive surface traction. Therefore, for consistency, it is necessary to determine the contact region under compressive traction in the JKR solution. In the JKR theory, the effect of adhesion on Hertzian contact is included by balancing the external work with the surface energy and the elastic strain energy. The JKR model accounts for the effects of contact pressure and adhesion only within the contact area. The general solution of the contact pressure $p(r)$ can be obtained as the superposition of a compressive contact stress distribution due to the applied normal (compressive) force P_1 and an adhesive (tensile) contact stress distribution due to a tensile force P_2 applied by a rigid punch over the same contact radius (Eq. (A1)). Consequently, $p(r)$ is expressed as (Johnson, 1958)

$$p(r) = \frac{3P_1}{2\pi a^2}\left[1 - \left(\frac{r}{a}\right)^2\right]^{1/2} - \frac{P_2}{2\pi a^2}\left[1 - \left(\frac{r}{a}\right)^2\right]^{-1/2} \tag{A4}$$

where r is the radial distance from the center of contact.

The Hertzian contact load P_1 and the repulsive load P_2 at the instant of $P_{\max}$ are given by

$$P_1 = \frac{4E^*}{3R} a^3 \tag{A5}$$

$$P_2 = P_1 + \frac{3}{2}\pi R\Delta\gamma = \frac{4E^*}{3R} a^3 + \frac{3}{2}\pi R\Delta\gamma \tag{A6}$$

Substitution of Eqs. (A5) and (A6) into Eq. (A4) and use of the normalization $\bar{a} = a/(\varepsilon R)^{1/2}$ leads to the following equation of the normal stress distribution:

$$p(r) = \frac{2E^* a}{\pi R\left[1-\left(\frac{r}{a}\right)^2\right]^{1/2}}\left[\frac{2}{3} - \left(\frac{r}{a}\right)^2 - \frac{3\pi}{8\bar{a}^3}\left(\frac{R\Delta\gamma^{1/2}}{E^{*2}\varepsilon^3}\right)\right] \tag{A7}$$

Substitution of Eq. (A3) into Eq. (A7) yields,

$$p(r) = \frac{2E^* a}{\pi R\left[1-\left(\frac{r}{a}\right)^2\right]^{1/2}}\left[\frac{1}{3} - \left(\frac{r}{a}\right)^2\right] \tag{A8}$$

The contact radius a_c corresponding to the region of compressive surface traction, obtained by setting Eq. (A8) equal to zero, is given by $a_c = a/\sqrt{3}$. Hence, using Eq. (A3), the dimensionless contact radius $\bar{a}_c$ can be expressed as

$$\bar{a}_c = \frac{1}{\sqrt{3}}\bar{a} = \frac{1}{\sqrt{3}}\left(\frac{9\pi}{8}\right)^{1/3}\mu^{1/2} \approx 0.88\mu^{1/2} \quad \text{(A9)}$$

Nomenclature

A	contact area
$\bar{A}$	dimensionless contact area ($= A/\varepsilon R$)
A_H	contact area obtained from Hertz analysis
$\bar{A}_H$	dimensionless contact area obtained from Hertz analysis ($= A_H/\varepsilon R$)
A_o	apparent contact area
a	Hertzian contact radius
$\bar{a}$	dimensionless Hertzian contact radius ($= \bar{a}/(\varepsilon R)^{1/2}$)
a_c	contact radius
$\bar{a}_c$	dimensionless contact radius ($= a_c/(\varepsilon R)^{1/2}$)
d	mean surface separation
$\tilde{d}$	dimensionless mean surface separation ($= d/\sigma$)
E_1, E_2	elastic modulus of asperity (surface) 1 and 2, respectively
E^*	effective elastic modulus
F	interfacial force
$\bar{F}$	dimensionless interfacial force ($= F/2\pi R A_0 \Delta\gamma\eta$)
$F_{\max}$	maximum attractive (adhesive) interfacial force or strength of adhesion
$\bar{F}_{\max}$	dimensionless maximum attractive interfacial force or strength of adhesion ($= F_{\max}/-2\pi R A_0 \Delta\gamma\eta$)
h_0	half-space elastic deflection at the center of the proximity region
$\bar{h}_0$	dimensionless half-space elastic deflection at the center of the proximity region ($= h_0/\varepsilon$)
N	total number of potentially contacting asperities

$N_1,\ N_2$	number of asperity contacts of rough surfaces without jump-in instabilities in the surface separation range dominated by attraction and repulsion, respectively
$N_3,\ N_4$	number of noncontacting and contacting asperities of rough surfaces without jump-in instabilities in the surface separation range dominated by attraction and repulsion, respectively
$N_5,\ N_6$	numbers of asperity contacts of rough surfaces with jump-in instabilities in the surface separation range dominated by attraction and repulsion, respectively
P	interfacial force
$\bar{P}$	dimensionless interfacial force ($= P/2\pi R\Delta\gamma$)
P_H	interfacial force obtained from Hertz analysis
$\bar{P}_H$	dimensionless interfacial force obtained from Hertz analysis ($= P_H/2\pi R\Delta\gamma$)
$P_{\max}$	maximum attractive (adhesion) force
$\bar{P}_{\max}$	dimensionless maximum attractive (adhesion) force ($= P_{\max}/2\pi R\Delta\gamma$)
P_{off}	pull-off force
$\bar{P}_{off}$	dimensionless pull-off force ($= P_{off}/2\pi R\Delta\gamma$)
P_1	normal (compressive) force in JKR model
P_2	rigid-punch adhesive (tensile) force in JKR model
p	pressure
R	reduced radius of curvature or asperity radius in rough-surface contact model
R_1, R_2	radius of curvature of asperity 1 and 2, respectively
S	total contact area
$\bar{S}$	dimensionless total contact area ($= S/RA_0\eta\varepsilon$)
r	horizontal (radial) coordinate (distance)
x	vertical coordinate or surface gap
x_o	minimum surface gap
$\bar{x}_o$	dimensionless minimum surface gap ($= x_o/\varepsilon$)
x_{oc}	minimum surface gap at the instant of jump-in
$\bar{x}_{oc}$	dimensionless critical minimum surface gap at the instant of jump-in ($= \bar{x}_{oc}/\varepsilon$)
z	asperity height
$\tilde{z}$	dimensionless asperity height ($= z/\sigma$)

Greek symbols

$\Delta\gamma$	work of adhesion
γ_1, γ_2	surface energy of asperity (surface) 1 and 2, respectively
γ_{12}	interfacial energy of asperities (surfaces) 1 and 2
δ_o	minimum surface separation
$\bar{\delta}_o$	dimensionless minimum surface separation ($= \delta_o/\varepsilon$)
δ_{oc}	critical minimum surface separation at the instant of maximum adhesion force
$\bar{\delta}_{oc}, \tilde{\delta}_{oc}$	dimensionless critical minimum surface separation at the instant of maximum adhesion force ($= \delta_{oc}/\varepsilon, \delta_{oc}/\sigma$)
δ_o^*	critical minimum surface separation at the instant of initial contact
$\bar{\delta}_o^*, \tilde{\delta}_o^*$	dimensionless critical minimum surface separation at the instant of initial contact ($= \delta_o^*/\varepsilon, \delta_o^*/\sigma$)
ε	equilibrium interatomic distance
ζ	ratio of surface roughness to equilibrium interatomic distance
η	area density of asperities
θ	adhesion parameter
μ	Tabor parameter
ν_1, ν_2	Poisson's ratio of asperity (surface) 1 and 2, respectively
ξ	general adhesion parameter
σ	root-mean-square (rms) surface roughness
σ_s	standard deviation of asperity heights
ϕ	asperity height distribution function
$\tilde{\phi}$	dimensionless asperity height distribution function
ω	ratio of standard deviation of asperity heights to surface roughness

References

Boussinesq, J., 1885. Application des potentiels à l' étude de l' équilibre et du mouvement des solides elastiques. Gauthier-Villars, Paris, France.

Bradley, R.S., 1932. The cohesive force between solid surfaces and the surface energy of solids. Philosophical Magazine 13, 853–862.

Carpick, R.W, Ogletree, D.F., Salmeron, M., 1999. A general equation for fitting contact area and friction vs load measurements. Journal of Colloid and Interface Science 211, 395–400.

Ciavarella, M., Greenwood, J.A., Paggi, M., 2008. Inclusion of "interaction" in the Greenwood and Williamson contact theory. Wear 265, 729–734.

Derjaguin, B.V., Muller, V.M., Toporov, Y.P., 1975. Effect of contact deformations on the adhesion of particles. Journal of Colloid and Interface Science 53, 314–326.

Du, Y., Chen, L., McGruer, N.E., Adams, G.G., Etsion, I., 2007. A finite element model of loading and unloading of an asperity contact with adhesion and plasticity. Journal of Colloid and Interface Science 312, 522–528.

Feng, J.Q., 2000. Contact behavior of spherical elastic particles: a computational study of particle adhesion and deformations. Colloids and Surfaces A: Physicochemical and Engineering Aspects 172, 175–198.

Feng, J.Q., 2001. Adhesive contact of elastically deformable spheres: a computational study of pull-off force and contact radius. Journal of Colloid and Interface Science 238, 318–323.

Fuller, K.N.G., Tabor, D., 1975. The effect of surface roughness on the adhesion of elastic solids. Proceedings of the Royal Society of London Series A 345, 327–342.

Greenwood, J.A., 1997. Adhesion of elastic spheres. Proceedings of the Royal Society of London Series A 453, 1277–1297.

Greenwood, J.A., 2009. Adhesion of small spheres. Philosophical Magazine 89, 945–965.

Greenwood, J.A., Williamson, J.B.P., 1966. Contact of nominally flat surfaces. Proceedings of the Royal Society of London Series A 295, 300–319.

Johnson, K.L., 1958. A note on the adhesion of elastic solids. British Journal of Applied Physics 9, 199–200.

Johnson, K.L., Kendall, K., Roberts, A.D., 1971. Surface energy and the contact of elastic solids. Proceedings of the Royal Society of London Series A 324, 301–313.

Kadin, Y., Kligerman, Y., Etsion, I., 2008. Loading–unloading of an elastic-plastic adhesive spherical microcontact. Journal of Colloid and Interface Science 321, 242–250.

Kesari, H., Doll, J.C., Pruitt, B.L., Cai, W., Lew, A.J., 2010. Role of surface roughness in hysteresis during adhesive elastic contact. Philosophical Magazine Letters 90, 891–902.

Kesari, H., Lew, A.J., 2011. Effective macroscopic adhesive contact behavior induced by small surface roughness. Journal of the Mechanics and Physics of Solids 59, 2488–2510.

Kim, K.-S., McMeeking, R.M., Johnson, K.L., 1998. Adhesion, slip, cohesive zones and energy fluxes for elastic spheres in contact. Journal of the Mechanics and Physics of Solids 46, 243–266.

Komvopoulos, K., Gong, Z.-Q., 2007. Stress analysis of a layered elastic solid in contact with a rough surface exhibiting fractal behavior. International Journal of Solids and Structures 44, 2109–2129.

Maugis, D., 1992. Adhesion of spheres: the JKR-DMT transition using a Dugdale model. Journal of Colloid and Interface Science 150, 243–269.

Maugis, D., 1996. On the contact and adhesion of rough surfaces. Journal of Adhesion Science and Technology 10, 161–175.

McCool, J.I., 1986. Comparison of models for the contact of rough surfaces. Wear 107, 37–60.

Morrow, C., Lovell, M., Ning, X., 2003. A JKR-DMT transition solution for adhesive rough surface contact. Journal of Physics D: Applied Physics 36, 534–540.

Mukherjee, S., Ali, S.M., Sahoo, P., 2004. An improved elastic–plastic contact model of rough surfaces in the presence of adhesion. Proceedings of the Institution of Mechanical Engineers, Part J: Journal of Engineering Tribology 218, 557–567.

Muller, V.M., Yushchenko, V.S., Derjaguin, B.V., 1980. On the influence of molecular forces on the deformation of an elastic sphere and its sticking to a rigid plane. Journal of Colloid and Interface Science 77, 91–101.

Sahoo, P., Chowdhury, S.K.R., 1996. A fractal analysis of adhesion at the contact between rough solids. Proceedings of the Institution of Mechanical Engineers, Part J: Journal of Engineering Tribology 210, 269–279.

Song, Z., Komvopoulos, K., 2011. Adhesion-induced instabilities in elastic and elastic–plastic contacts during single and repetitive normal loading. Journal of the Mechanics and Physics and Solids 59, 884–897.

Song, Z., Komvopoulos, K., 2013. Delamination of elastic film from elastic–plastic substrate during adhesive contact loading and unloading. International Journal of Solids and Structures 50, 2549–2560.

Tabor, D., 1977. Surface forces and surface interactions. Journal of Colloid and Interface Science 58, 2–13.

Wu, J.-J., 2008. Easy-to-implement equations for determining adhesive contact parameters with the accuracy of numerical simulations. Tribology Letters 30, 99–105.

Ye, N., Komvopoulos, K., 2003. Indentation analysis of elastic-plastic homogeneous and layered media: criteria for determining the real material hardness. ASME Journal of Tribology 125, 685–691.

List of Figures

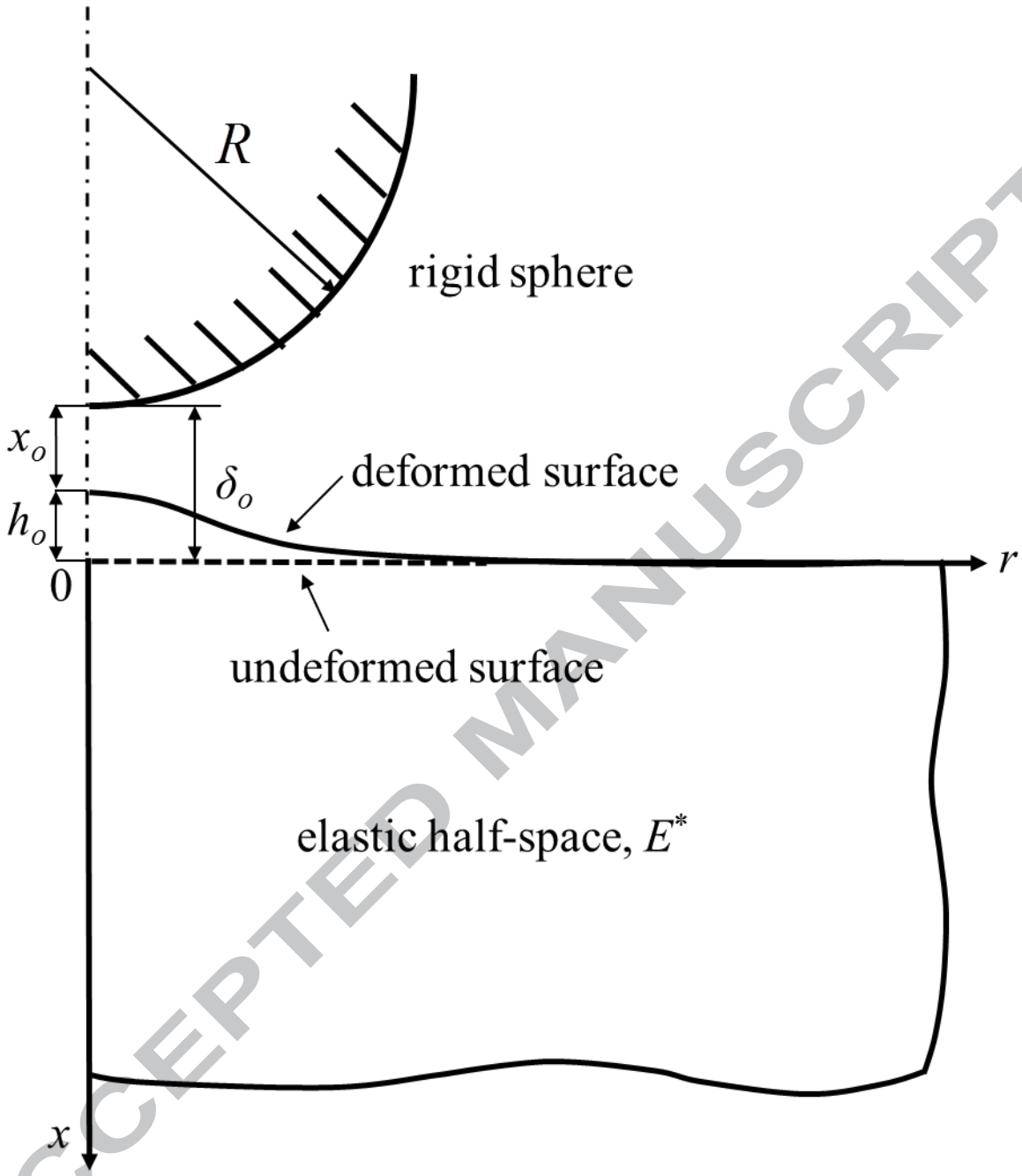

Figure 1

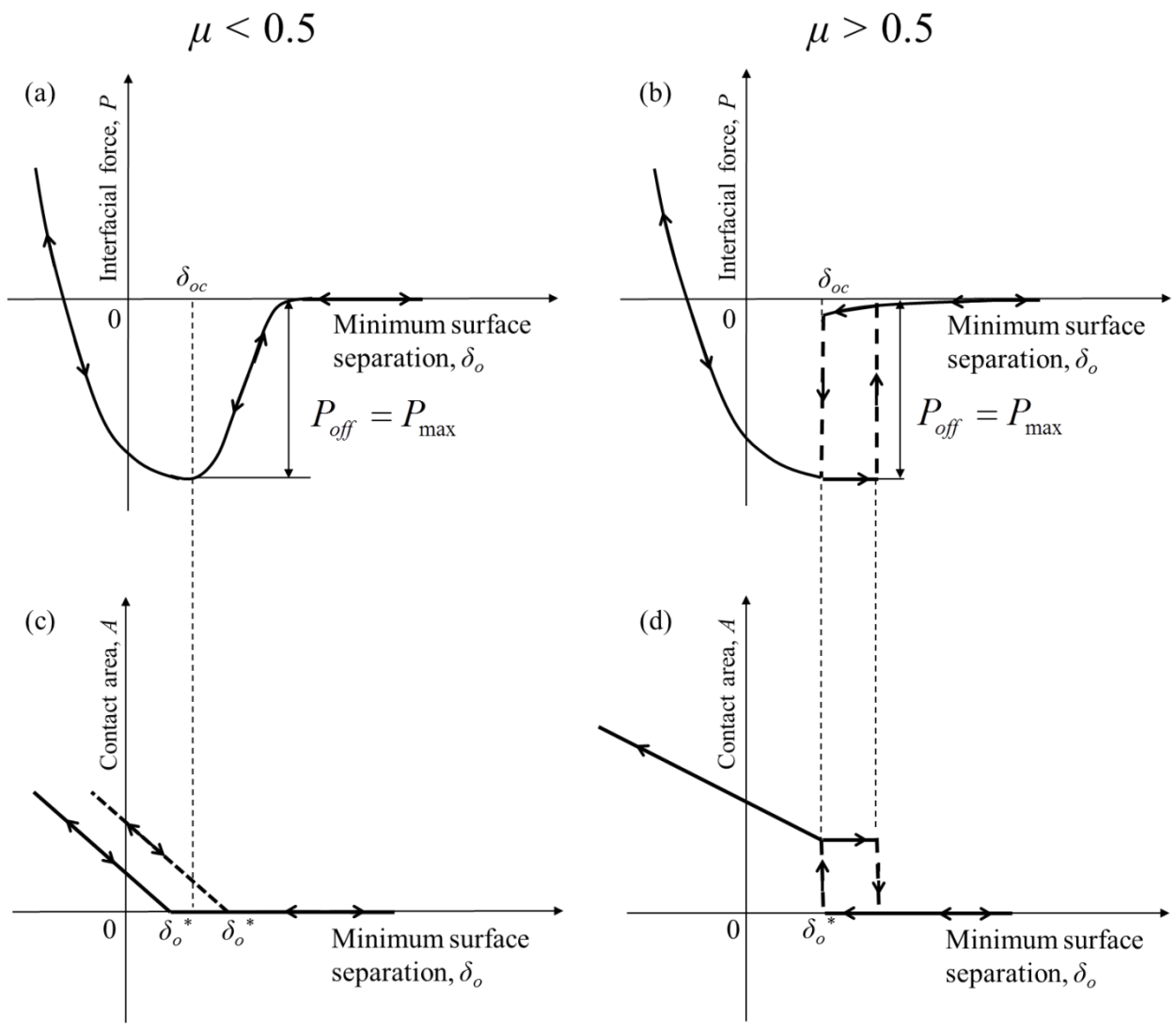
$\mu < 0.5$
$\mu > 0.5$
(a)
(b)
(c)
(d)
Interfacial force, P
Contact area, A
δ_{oc}
0
Minimum surface separation, δ_o
$P_{off} = P_{\max}$
δ_o^*

Figure 2

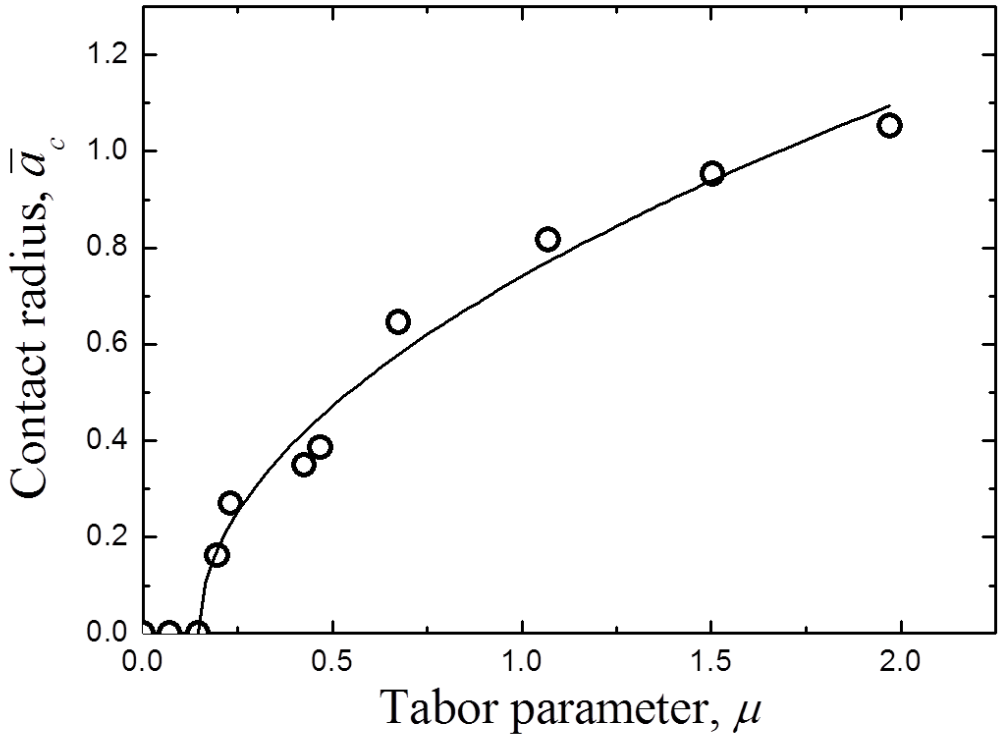
Contact radius, $\bar{a}_c$
1.2
1.0
0.8
0.6
0.4
0.2
0.0
0.0
0.5
1.0
1.5
2.0
Tabor parameter, μ

Figure 3

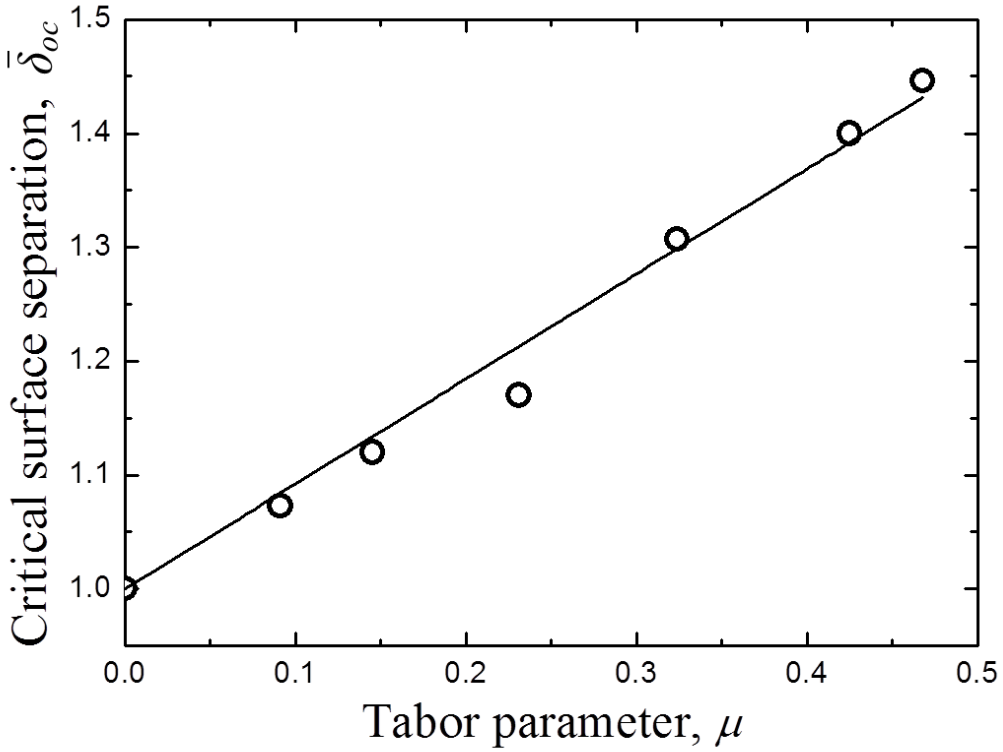
Critical surface separation, $\bar{\delta}_{oc}$
1.5
1.4
1.3
1.2
1.1
1.0
0.0
0.1
0.2
0.3
0.4
0.5
Tabor parameter, μ

Figure 4

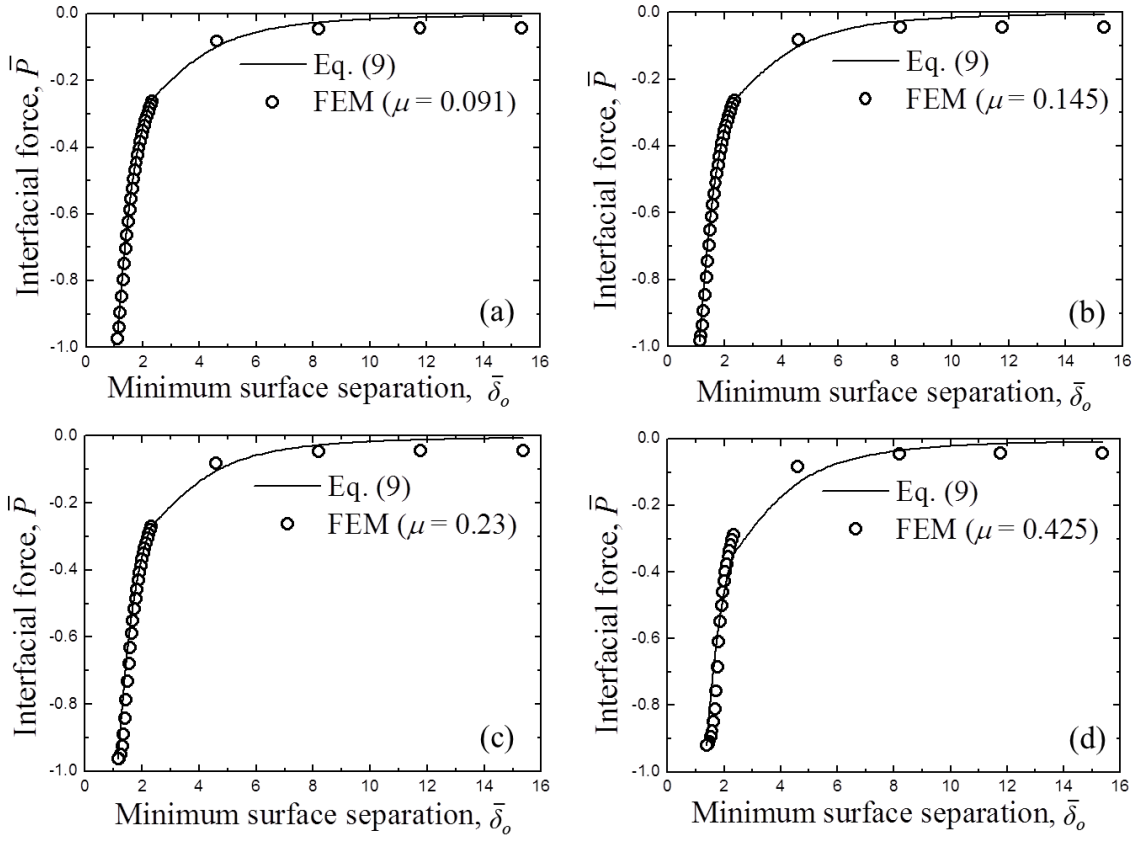
Interfacial force, $\bar{P}$
Minimum surface separation, $\bar{\delta}_o$
Eq. (9)
FEM (μ = 0.091)
(a)
FEM (μ = 0.145)
(b)
FEM (μ = 0.23)
(c)
FEM (μ = 0.425)
(d)

Figure 5

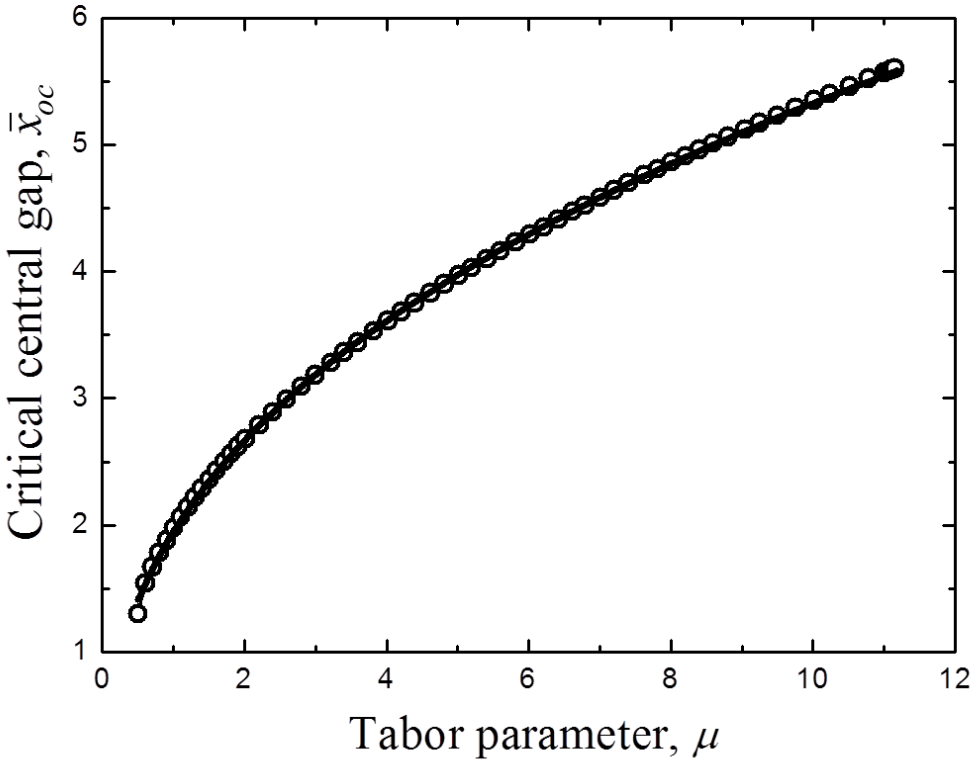
Critical central gap, $\bar{x}_{oc}$
Tabor parameter, μ
1
2
3
4
5
6
0
2
4
6
8
10
12

Figure 6

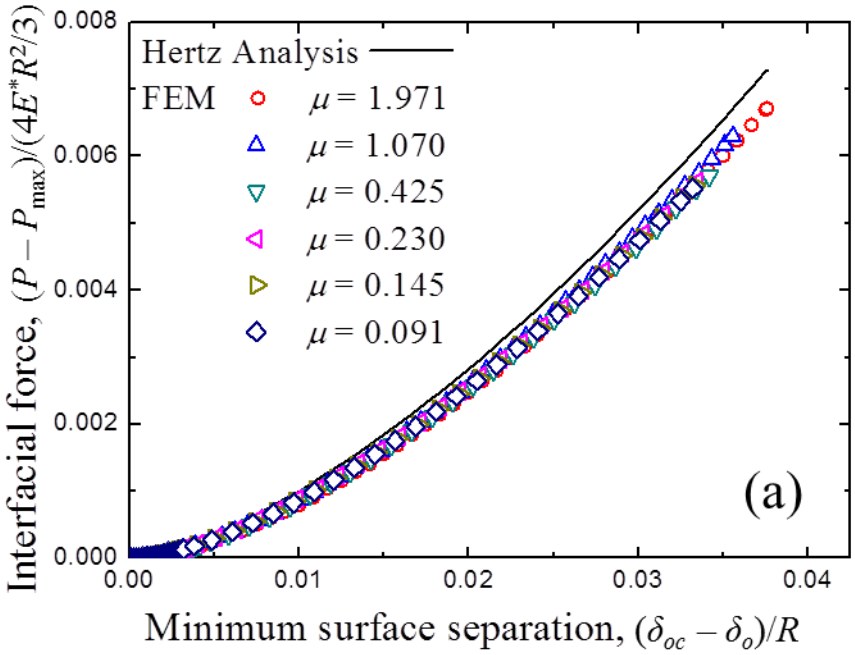
Hertz Analysis
FEM
$\mu = 1.971$
$\mu = 1.070$
$\mu = 0.425$
$\mu = 0.230$
$\mu = 0.145$
$\mu = 0.091$
(a)
Interfacial force, $(P - P_{max})/(4E^*R^2/3)$
Minimum surface separation, $(\delta_{oc} - \delta_o)/R$
0.000
0.002
0.004
0.006
0.008
0.00
0.01
0.02
0.03
0.04

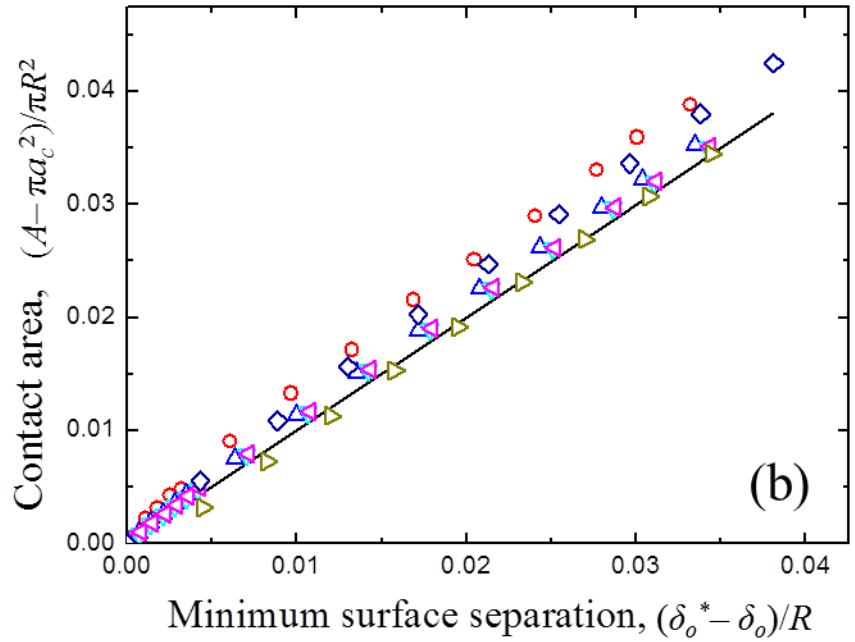
(b)
Contact area, $(A - \pi a_c^2)/\pi R^2$
Minimum surface separation, $(\delta_o^* - \delta_o)/R$
0.00
0.01
0.02
0.03
0.04

Figure 7

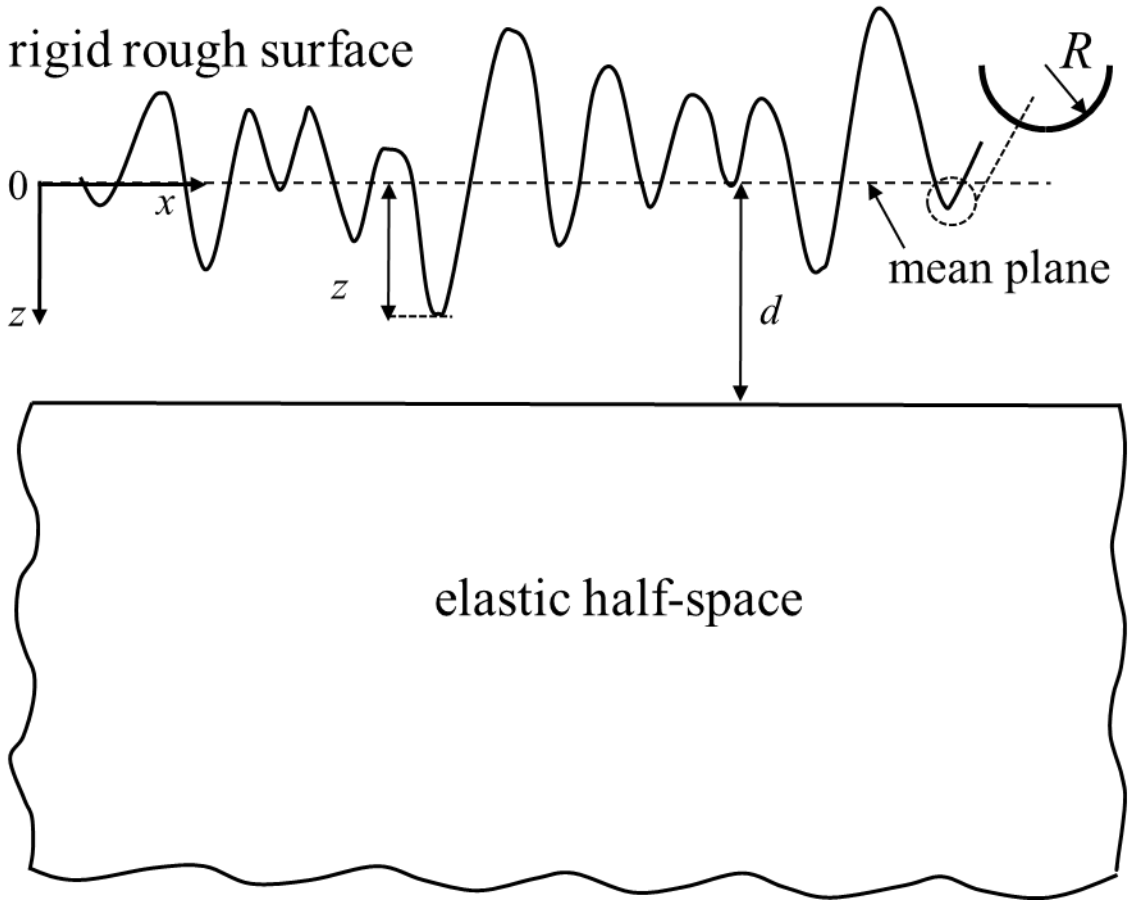

Figure 8

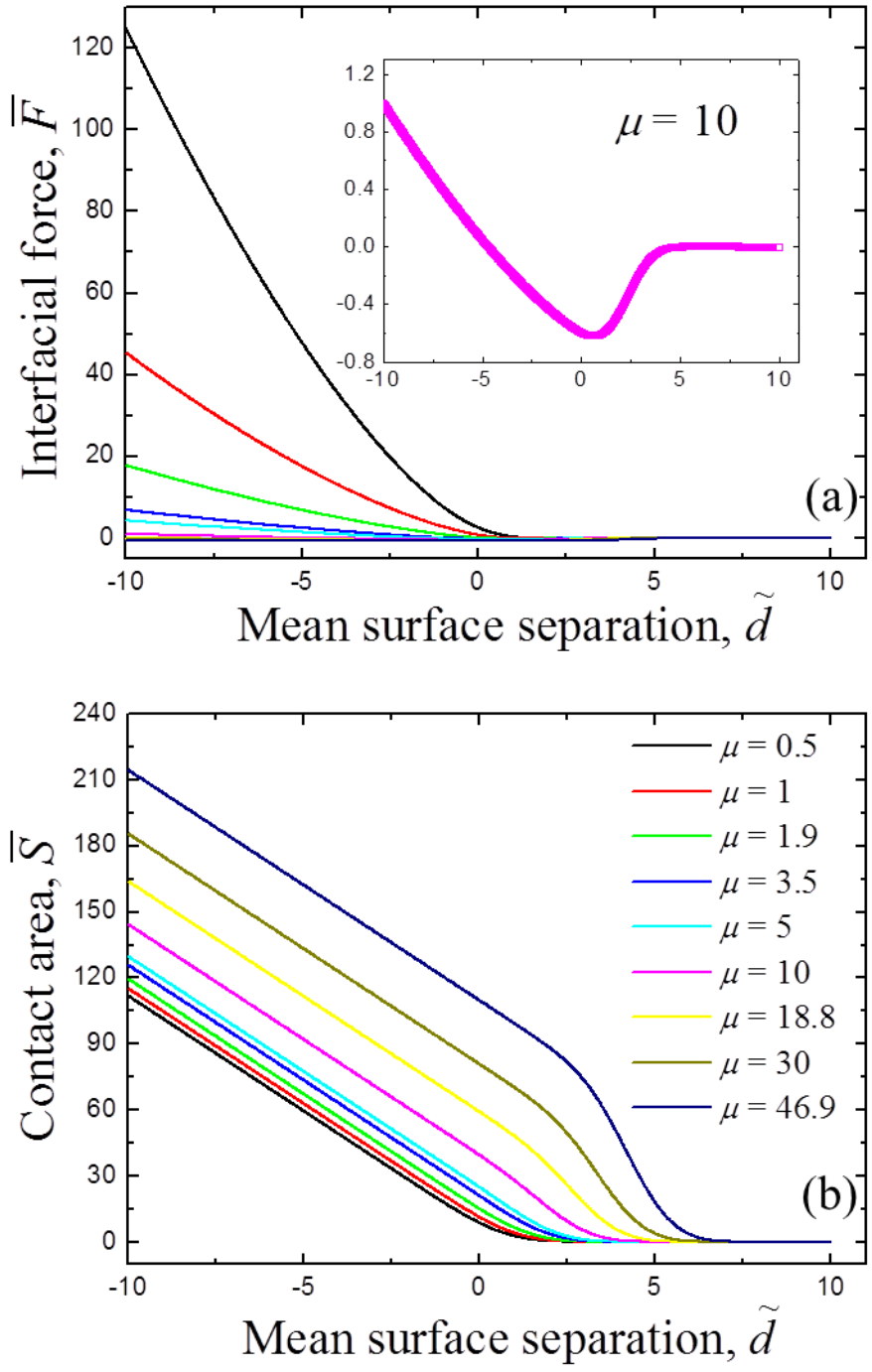
Interfacial force, $\overline{F}$
Mean surface separation, $\tilde{d}$
$\mu = 10$
(a)
Contact area, $\overline{S}$
Mean surface separation, $\tilde{d}$
$\mu = 0.5$
$\mu = 1$
$\mu = 1.9$
$\mu = 3.5$
$\mu = 5$
$\mu = 10$
$\mu = 18.8$
$\mu = 30$
$\mu = 46.9$
(b)

Figure 9

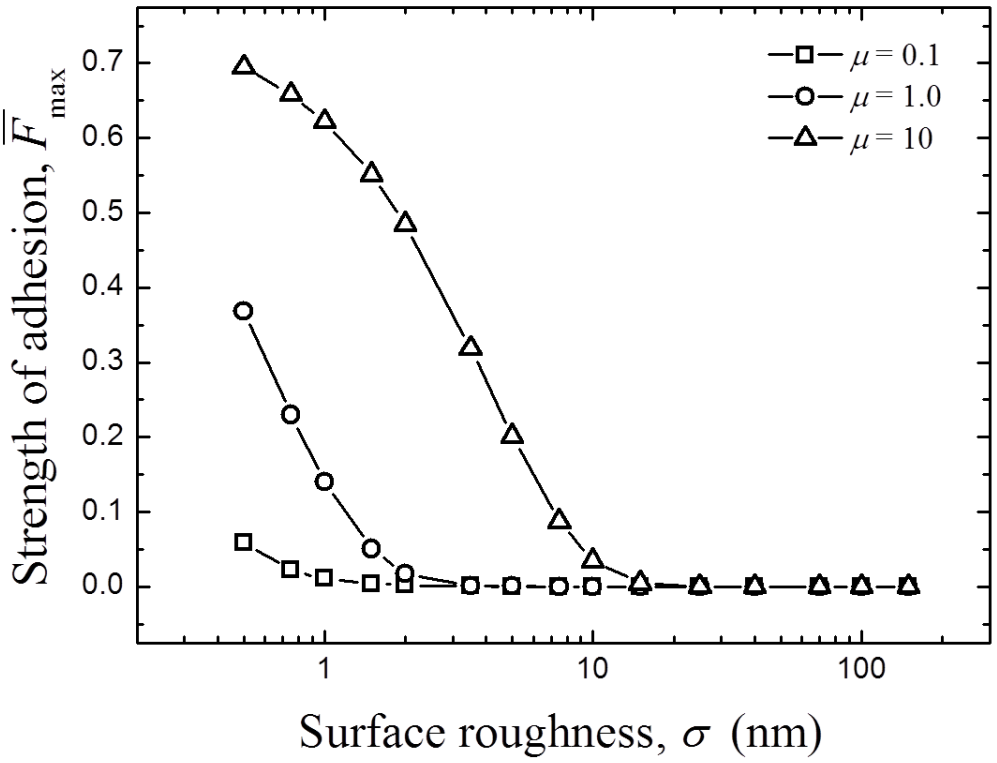
Strength of adhesion, $\overline{F}_{max}$
0.0
0.1
0.2
0.3
0.4
0.5
0.6
0.7
1
10
100
Surface roughness, σ (nm)
μ = 0.1
μ = 1.0
μ = 10

Figure 10

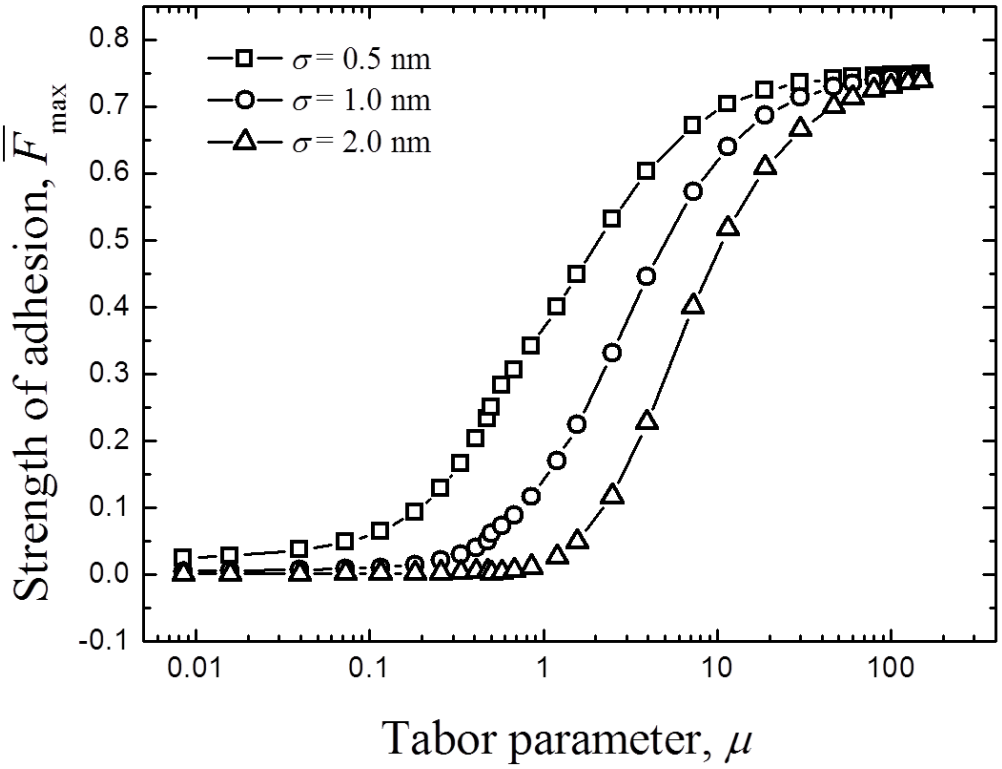
σ = 0.5 nm
σ = 1.0 nm
σ = 2.0 nm
Strength of adhesion, $\overline{F}_{max}$
Tabor parameter, μ
0.8
0.7
0.6
0.5
0.4
0.3
0.2
0.1
0.0
-0.1
0.01
0.1
1
10
100

Figure 11

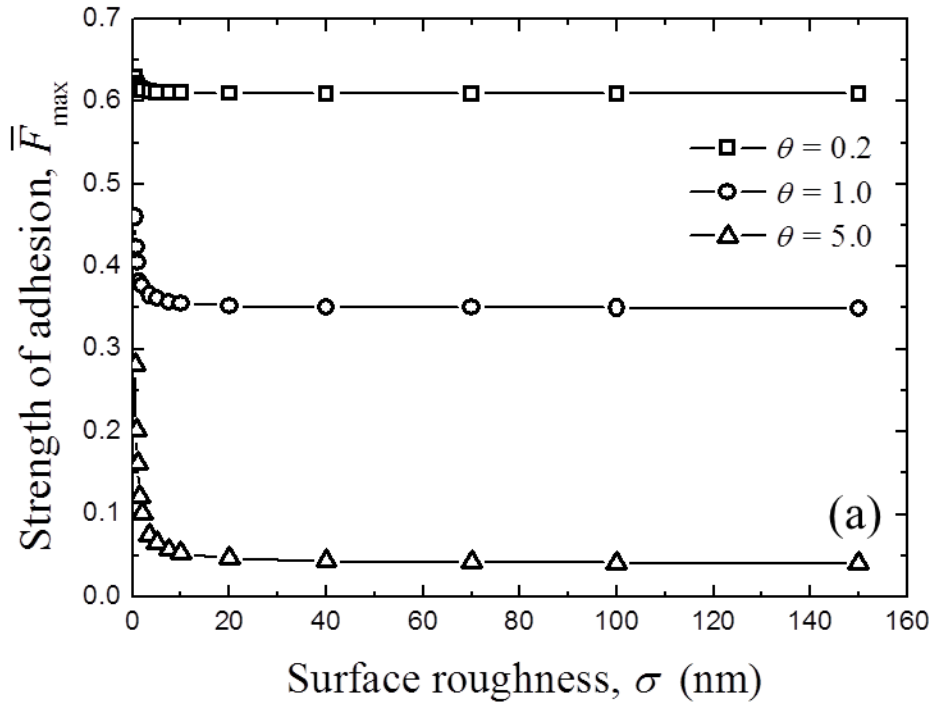
Strength of adhesion, $\overline{F}_{max}$
0.0
0.1
0.2
0.3
0.4
0.5
0.6
0.7
0
20
40
60
80
100
120
140
160
Surface roughness, σ (nm)
$\theta = 0.2$
$\theta = 1.0$
$\theta = 5.0$
(a)

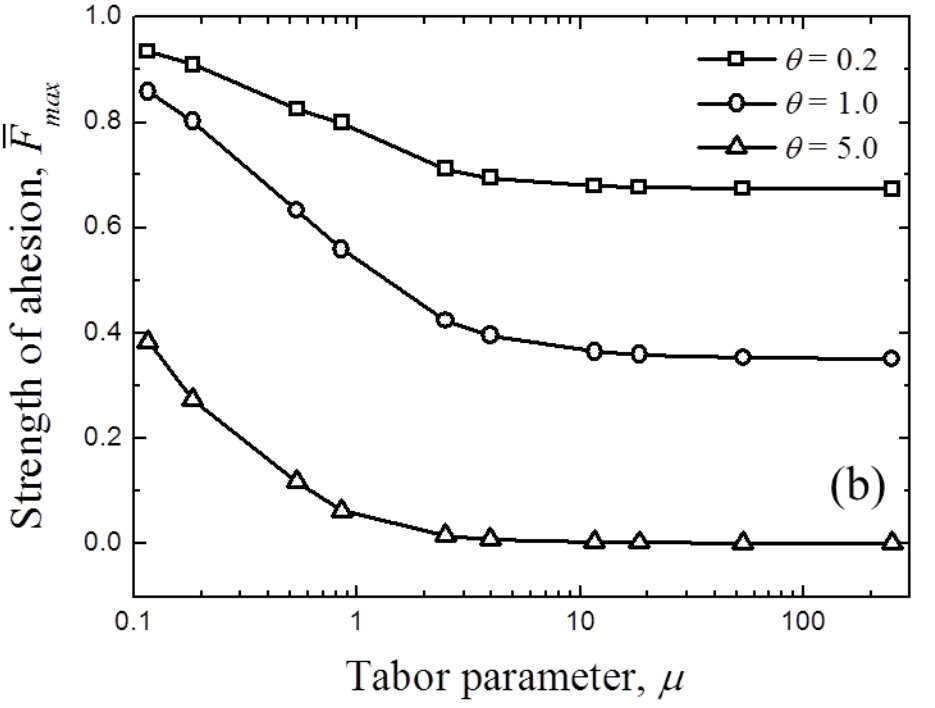
Strength of ahesion, $\overline{F}_{max}$
0.0
0.2
0.4
0.6
0.8
1.0
0.1
1
10
100
Tabor parameter, μ
$\theta = 0.2$
$\theta = 1.0$
$\theta = 5.0$
(b)

Figure 12

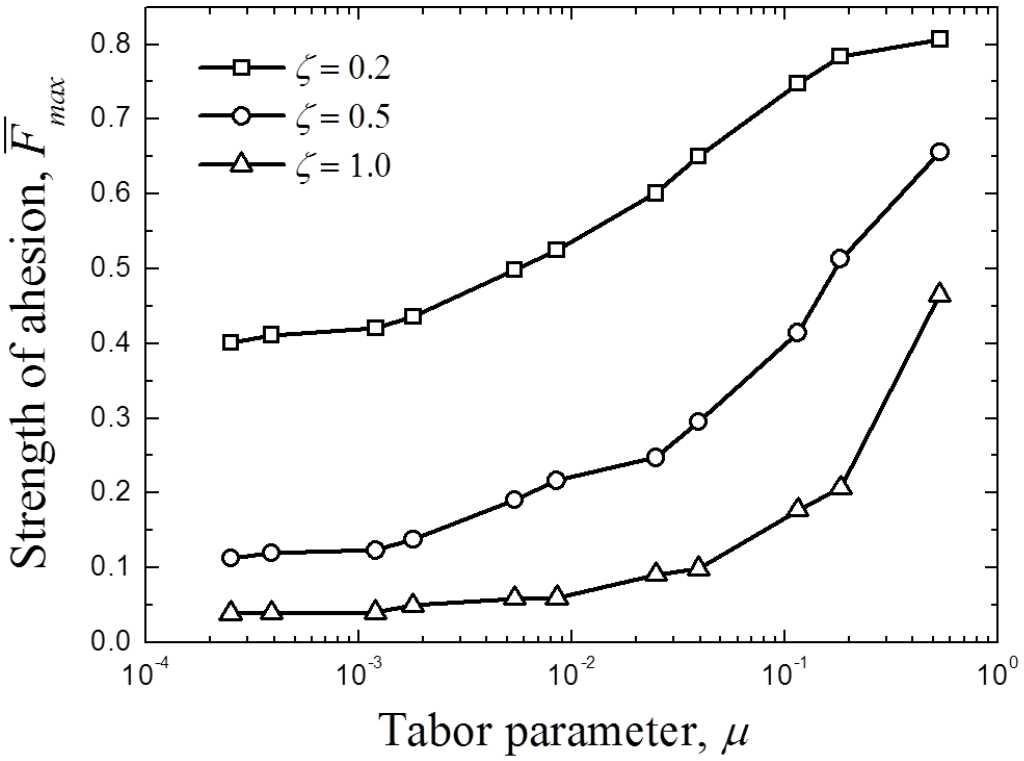
Strength of ahesion, $\overline{F}_{max}$
0.0
0.1
0.2
0.3
0.4
0.5
0.6
0.7
0.8
$\zeta = 0.2$
$\zeta = 0.5$
$\zeta = 1.0$
10^{-4}
10^{-3}
10^{-2}
10^{-1}
10^{0}
Tabor parameter, μ

Figure 13